Tomographic Determination of the Spatial Distribution of Water Vapor Using GPS Observations

M. Troller[1], A. Geiger[1], E. Brockmann[2], J.-M. Bettems[3], B. Bürki[1], H.-G. Kahle[1]

[1] *Institute of Geodesy and Photogrammetry, Swiss Federal Institute of Technology, Zürich, Switzerland*

[2] *Swiss Federal Office of Topography, Geodetic bases and permanent networks, Wabern, Switzerland*

[3] *Federal Office of Meteorology and Climatology, Zürich, Switzerland*

1 Introduction

GPS meteorology is a promising technique to estimate the total amount of water vapor in the troposphere on a continuous basis using satellite navigation systems, (e.g. Bevis et. al., 1992). With GPS tomography, it is aimed at determining also the vertical distribution of water vapor in the troposphere with a high temporal resolution (e.g. Flores et. al., 2000; Hirahara, 2000; Kruse, 2001; Troller, 2004). In this study, hourly resolution has been investigated, which represents a major improvement compared to time resolution obtained from operational ballon soundings.

2 Principle of GPS Tomography

GPS signals are significantly influenced by the atmosphere, especially the ionosphere and troposphere, along their path from the satellite to the GPS antenna. The satellites are transmitting at two different carrier frequencies in the radio L-band. As the ionosphere is a dispersive medium in the radio frequency range, its influence can be eliminated by composing a linear combination of the two GPS carrier frequencies. The remaining effect is caused by the delay of the signal due to the refractivity of the troposphere. Furthermore, this effect can be subdivided into a so-called dry and wet part, the latter being proportional to the integrated precipitable water vapor (e.g. Hofmann-Wellenhof et. al., 2001).

The main advantages of GPS are that

1. measurements can be carried out on a continuous basis at relatively low expense
2. GPS is an all-weather observing system, allmost insensitive to clouds, and the effect of liquid water can usually be neglected (Elgered, 1993).

The wet propagation delay Δ_{wet}^{PD} of a radio signal from the satellite to the receiver antenna is defined as:

$$\Delta_{wet}^{PD} = \int_{antenna}^{satellite} (n_{wet} - 1)\, ds = 10^{-6} \int_{antenna}^{satellite} N_{wet} ds \tag{1}$$

n_{wet} represents the refractive index due to water vapor and N_{wet} the wet refractivity whereby latter is defined as $N_{wet} = 10^6 \cdot (n_{wet} - 1)$; ds is the length of a ray path element. The ray bending effect can be neglected, as the cutoff angle of 10 degrees (Mendes, 1999) has been applied throughout the presented evaluation.

However, the wet path delay reflects the integrated amount of water vapor, only. To achieve the spatial distribution, a tomographic approach was investigated. In the tomographic approach, a discretization of the atmosphere with a voxel model is used. The number of layers and the horizontal and vertical size of voxels are correspondingly defined. Ellipsoidal boundary surfaces of the layers account for the earth's curvature. At the horizontal boundaries in each layer open voxels are added, i.e., these voxels reach ad infinitum. Consequently, no rays are neither completely nor partially outside the model. Within each voxel, the wet refractivity N_{wet} is introduced as an unknown constant. Discretizing (1), the wet slant path delay from satellite r to receiver antenna p as observed is related to the unknowns (refractivity N_{wet}) as follows:

$$\Delta_{wet,p}^{PD,r} = 10^{-6} \cdot \sum_{i=1}^{k} N_{wet,i}\, \Delta s_{i,p}^{\ r} \tag{2}$$

where, $\Delta s_{i,p}^{\ r}$ represents the length of the path through voxel i, and k the number of voxels. Wet slant path delays can be derived from several remote sensing techniques such as GPS, water vapor radiometry and solar spectrometry. In the current approach, we focus on GPS double difference path delays. By following the well established concept of double differencing (e.g. Beutler et. al., 2001), we obtain from (2) the double difference wet slant path delays $\Delta_{\ wet,pq}^{2,PD,rs}$ of the satellites r and s and the stations p and q:

$$\Delta_{\ wet,pq}^{2,PD,rs} = (\Delta_{wet,q}^{PD,r} - \Delta_{wet,p}^{PD,r}) - (\Delta_{wet,q}^{PD,s} - \Delta_{wet,p}^{PD,s}) \tag{3}$$

The following approach has been applied to retrieve the double difference path delays: GPS data have been processed using the Bernese GPS Software (Beutler et. al., 2001) yielding GPS zenith path delays $\overline{\Delta^{PD}}$ and double difference phase residuals $\Delta^2\Phi$ as processing output. The double difference path delays $\Delta_{\ pq}^{2,PD,rs}$ of the satellites r, s and the stations p, q are reconstructed from the GPS-derived zenith path delays $\overline{\Delta_p^{PD}}, \overline{\Delta_q^{PD}}$, which have to be mapped back to the corresponding elevations using the corresponding mapping functions (airmass factors) $m(el_p^r), m(el_q^r), m(el_p^s), m(el_q^s)$. Furthermore, the double difference phase residual $\Delta^2\Phi_{pq}^{rs}$ is added:

$$\Delta_{\ pq}^{2,PD,rs} = \overline{\Delta_{\ pq}^{2,PD,rs}} + \Delta^2\Phi_{pq}^{rs} \tag{4}$$

where:

$$\begin{aligned}\overline{\Delta_{\ pq}^{2,PD,rs}} = {} & (\overline{\Delta_q^{PD}} \cdot m(el_q^r) - \overline{\Delta_p^{PD}} \cdot m(el_p^r)) - \\ & (\overline{\Delta_q^{PD}} \cdot m(el_q^s) - \overline{\Delta_p^{PD}} \cdot m(el_p^s))\end{aligned} \tag{5}$$

Using ground meteorological measurements, the zenith dry path delay can be determined by applying the formula of Saastamoinen (Saastamoinen, 1972; Troller, 2004). Subsequently, the double difference dry slant path delay has been constructed using the same approach as in (5). Finally, the wet part of the double difference slant path delay $\Delta_{\ wet,pq}^{2,PD,rs}$ is extracted by subtracting the dry part from the total amount.

The number of traversing rays per voxel depends on the geometry defined by the number of visible satellites, the distribution of the ground stations and the size of the voxels. GPS-tomography usually generates a partly ill-posed problem in the sense that only a portion of the unknowns (refractivity per voxel) can be determined whereas the other part is under-determined. Additional information is necessary to solve the equation system. In this approach, the uppermost layer is bounded by 8.000 m and 15.000 m lower and upper

level, respectively. This allows for the assumption of a priori values of $N_{wet} = 0\,ppm$ in that level. In special cases, a priori values can be introduced for other voxels. This procedure is described in Section 4. In addition, the voxels are mutually coupled by using a realistic covariance function to limit the variation of the difference in refractivity of neighboring voxels. However, only direct neighboring voxels are correlated to allow for steep refractivity gradients.

Extensive simulations using various weather conditions show the feasibility of this approach and indicate the need of double difference measurements with noise not exceeding 5 mm (Troller et. al., 2002). By properly treating the GPS data a double difference noise limit of 4-5 mm can be achieved in most cases, thus allowing for a tomographic solution with sufficient accuracy.

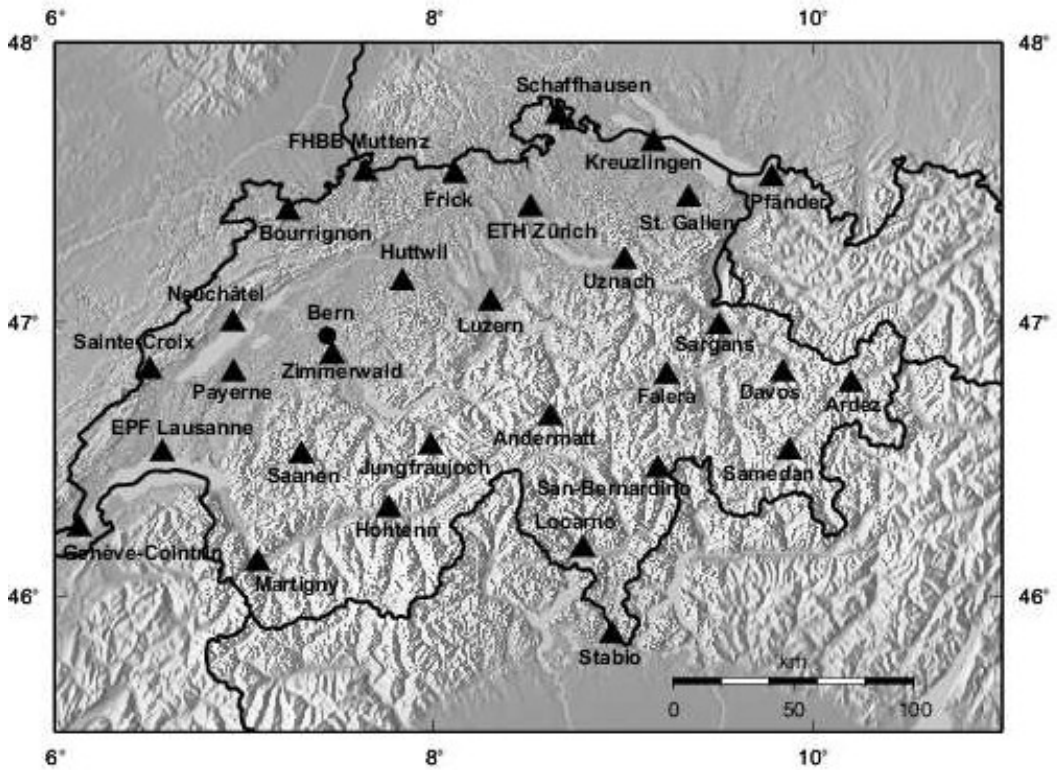

Figure 1: GPS stations of the Swiss Permanent GPS Reference Network AGNES (swisstopo). The network contains 30 AGNES stations, with a height distribution from 400 - 3.600 m. For the automated processing, 20 EUREF stations and 23 stations from other networks are included. The figure shows the stations of the Swiss territory only.

3 Description of the Experiment

The observations have been carried out in Switzerland. The data used are collected in the Swiss permanent GPS reference network (AGNES) of swisstopo. It covers the entire Swiss territory with a dense horizontal and vertical resolution (Fig. 1). Large height differences between the GPS stations are suitable for an accurate tomographic solution. An automated near real-time processing provides hourly means of zenith total delays, which are then used to derive instantaneous values of GPS path delays.

Data of the meteorological network ANETZ of MeteoSwiss (SMA, 1985) is used to decompose the total delays in its wet and dry part. ANETZ contains a total of 72 well distributed ground stations covering Switzerland and allows an accurate splitting of the zenith total delay.

A period of one week in November 2002 was chosen for the investigations. Rapid weather changes, heavy rainfall, clear conditions and sunny periods occurred during that week.

The voxel model above the Swiss territory is chosen with 6×3 voxels in horizontal (voxel side lengths $\sim 50\,km$) and 16 layers up to 15.000 m (Fig. 2). Water vapor profiles are retrieved on an hourly basis.

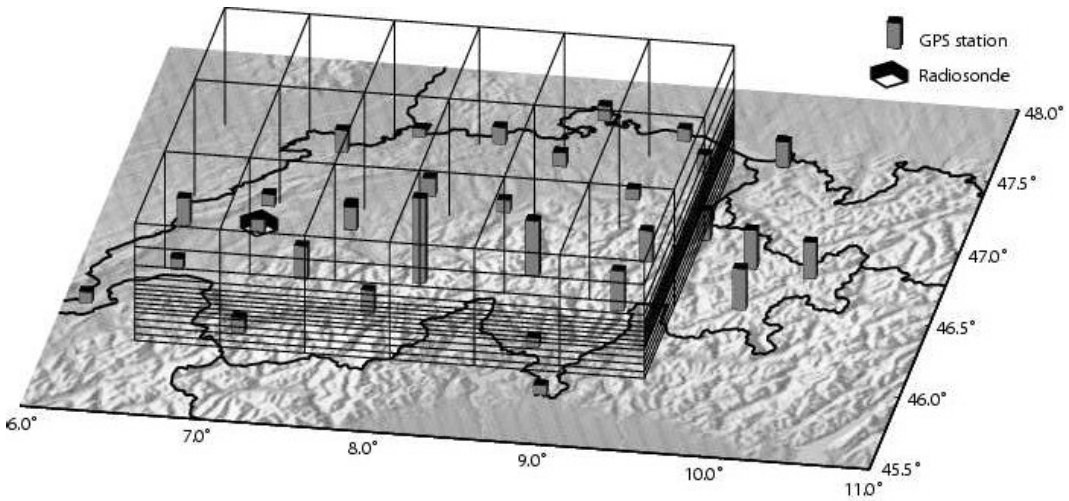

Figure 2: 3D view of the evaluation perimeter. The tomographic voxel model consists of 16 layers up to 15.000 m height. The borders of the layers are set at 0 m, 200 m, 600 m, 900 m, 1.200 m, 1.400 m, 1.600 m, 1.800 m, 2.000 m, 2.200 m, 2.400 m, 2.700 m, 3.200 m, 4.000 m, 5.000 m, 8.000 m, 15.000 m (the figure shows layers up to 5.000 m height only). Each layer contains 6 voxels in longitude and 3 voxels in latitude (spacing 0.5°) plus 22 outer voxels (not shown on the figure). The GPS stations are shown as column according to their station height. Radiosondes are launched from the radiosonde station Payerne (MeteoSwiss), shown as cuboid.

The tomographic results are compared with data of the operational high resolution NWP model of MeteoSwiss (aLMo).

4 Profile Determination and Evaluation

Double difference residuals and hourly means of zenith path delays are determined using the Bernese software package (Beutler et. al., 2001). Reconstructed double-difference wet slant delays are then introduced into the tomographic software package AWATOS.

Two types of tomographic profiles are determined, containing different constraints. On one hand, *AWATOS Correlation* includes inter-voxel constraints between all neighboring voxels. Compared to a double-difference observation, the constraints are down-weighted by a factor of 50^2 (regularization factor = $\frac{1}{2500}$). In addition, an a priori wet refractivity of zero is assigned to the uppermost layer (8.000-15.000 m) with a regularization factor of $\frac{1}{900}$. On the other hand, *AWATOS ANETZ* contains the same constraints as *AWATOS Correlation* and in addition one a priori wet refractivity value for each voxel lower than 2000 m. These

refractivity values are based on a collocation and interpolation procedure (COMEDIE software package, Troller et. al., 2000) using the operationally available meteorological ground station data (ANETZ, MeteoSwiss).

The least-squares adjustment of the tomographic equation system yields the matrices of the cofactors of the unknown parameters from the inverted normal matrices (e.g. Mikhail, 1976). The comparison of the two cofactor matrices of the two solutions reveals the impact on quality of the two different types of solution. The a priori calculation takes no measurements into account. It assesses the geometry and the weighting of the measurements, only. The solution *AWATOS Correlation* shows a slight increase of the precision with height. Regarding the solution *AWATOS ANETZ*, a significant improvement of the square root of cofactors is visible in the first 2.000 m height but also in the higher voxels (Fig. 3).

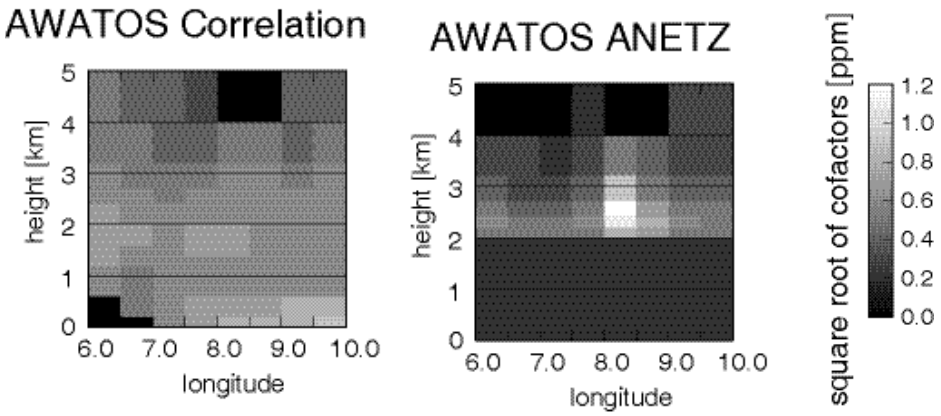

Figure 3: Cross section of the square root of cofactors at latitude 46.75°. The two top layers (5.000 - 15.000 m height) are not shown in the figures. (a) represents the situation of the solution *AWATOS Correlation* and (b) *AWATOS ANETZ*. It is seen, that if a priori refractivity is introduced, the precision increases significantly.

In Fig. 4, two examples of tomographic profiles, aLMo data and radiosonde profiles are displayed. Furthermore, the profile obtained with COMEDIE is plotted. The lowermost 2.000 m of the latter profile are used to constrain the solution *AWATOS ANETZ*. The comparison of the profiles confirms the conclusions made of the matrices of cofactors: The degree of agreement of the individual profiles is varying. *AWATOS ANETZ* fits always more accurately to aLMo than *AWATOS Correlation*. The 22 radiosonde launches during the investigation week at station Payerne have been used to perform a comparison to the tomographic profiles and the aLMo model (Table 1). The conclusion of Fig. 4 can be verified, the mean rms of *AWATOS ANETZ* is half as large as of *AWATOS Correlation*. Fig. 5 shows the mean rms of the tomographic profiles compard to the radiosondes as function of the height. The impact of the a priori refractivity in the first 2000 m height is clearly visible.

The comparison of aLMo to the radiosonde profiles is also documented in Table 1. The agreement is within 2.6 *ppm* (refractivity units) at station Payerne, where radiosondes are available to compare the aLMo model.

As radiosondes are available every six or twelf hours and at the station Payerne only, the aLMo data with an hourly resolution have been used to compare the tomographic solutions over entire Switzerland. Thus, a total of 3024 profiles are compared to aLMo for the one-week measurements (Fig. 6). In Fig. 4, two profiles with different levels of agreement, mainly depending on the atmosphere's actual state are shown. This behavior can be confirmed by

Table 1: Statistical analysis of the tomographic profiles and aLMo compared to the radiosondes. The analysis contains 22 profiles. The accuracy of the two tomographic solutions varies significantly. The mean rms of AWATOS Correlation is approximately double as the coresponding value of AWATOS ANETZ. Furthermore, the latter has no significant mean offset.

	AWATOS Correlation	AWATOS ANETZ	aLMo[1]
mean offset	-6.3	-1.4	0.5
mean rms	12.7	5.1	2.6
mean σ	11.0	4.9	2.6

[1] aLMo data for the lowermost voxel (200 - 600 m height) are not available.

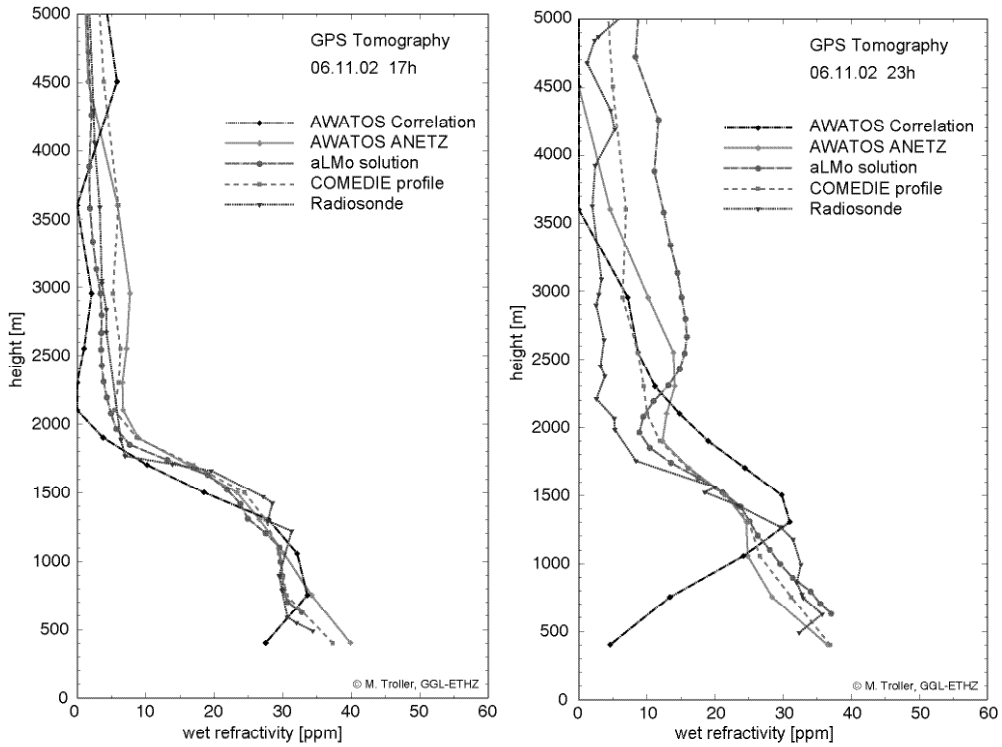

Figure 4: Wet refractivity profiles of the two tomographic solutions, the radiosonde ascending at the station Payerne (MeteoSwiss), data of the numerical weather model aLMo (MeteoSwiss) and the COMEDIE profile. (a) shows a profile with a steep refractivity gradient at 1.800 m height. All solutions match accurately together on the order of 10 ppm. (b) shows a situation with an inhomogeneous decrease of refractivity with height. *AWATOS Correlation* underestimates the wet refractivity in the lowest 1.000 m height. However, also the other tomographic solution as well as the radiosonde show differences to the aLMo solution.

inspecting the time series analysis of Fig. 6. Periods with large rms on November 3, 6 and 9, coincide with atmospheric situations rapidly changing from heavy rain to dry periods and contrariwise. During these time periods, the differences between GPS-tomography and aLMo are larger. This may mainly be caused by the temporal averaging during each data assimilation period, thus neglecting gradients in time for the assimilation interval.

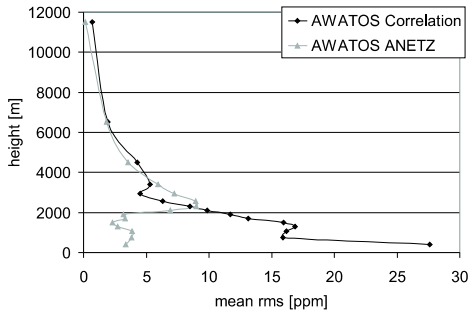

Figure 5: Mean rms of the two tomographic solutions compared to the radiosondes as a function of the height. The plot shows the comparison of the 22 radiosonde launches during the investigation week at the station Payerne. Generally, the rms is decreasing with increasing height. The impact of the a priori profiles on the first 2000 m height from COMEDIE is clearly visible in the solution AWATOS ANETZ.

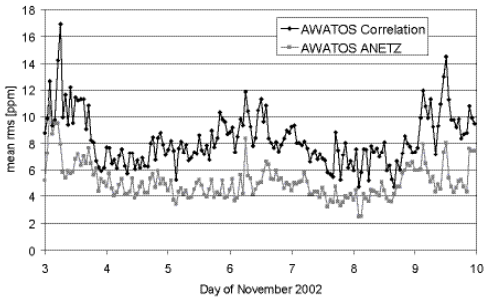

Figure 6: Time series of the mean of all profiles compared to aLMo. Overall, *AWATOS ANETZ* has a smaller rms than *AWATOS Correlation*. Three jumps are visible on November 3, 6 and 9.

5 Conclusions

The tomographic approach was successfully performed to process GPS data for the determination of 4 dimensional water vapor data.

Regularization methods are necessary to achieve a stable tomographic solution. Inter-voxel constraints and a priori refractivity information allow usually to achieve a high accuracy. An overall rms of about 5-8 *ppm* (refractivity units) or 0.8-1.3 $\frac{g}{m^3}$ absolute humidity compared to aLMo has been reached, depending on the tomographic solution. Using a temporal resolution of one hour, the accuracy remains approximately stable during the whole week, at least for the solution *AWATOS ANETZ*. Only during rapidly changing atmospheric situations, the rms is slightly decreasing. Further investigations showed (Troller, 2004) that the accuracy achieved at station Payerne, can be expected in whole Switzerland.

References

Beutler, G., Bock, H., Brockmann, E., Dach, R., Fridez, P., Gurtner, W., Hugentobler, U., Ineichen, D., Johnson, J., Meindl, M., Mervart, L., Rothacher, M., Schaer, S., Springer, T., and Weber, R., 2001. Bernese GPS software version 4.2. Edited by U. Hugentobler, S. Schaer and P. Fridez. Astronomical Institute, University of Berne.

Bevis, M., Businger, S., Herring, T., Rocken, C., Anthes, R., and Ware, R., 1992. GPS meteorology: Remote sensing of atmospheric water vapor using the global positioning system. *J. of Geophysical Research*, 97(D14), pp. 15787-15801.

Elgered, G. (1993). *Atmospheric Remote Sensing by Microwave Radiometry*, chapter Tropospheric Radio-Path Delay from Ground-based Microwave Radiometry, pp. 215–258. John Wiley and Sons, Inc.

Flores, A., Ruffini, G., and Rius, A., 2000. 4d tropospheric tomography using GPS slant wet delays. *Ann. Geophysicae*, 18, pp. 223-234.

Hirahara, K. 2000. Local GPS tropospheric tomography. *Earth Planets Space*, 52, pp. 935-939.

Hofmann-Wellenhof, B., Lichtenegger, H., and Collins, J., 2001. GPS Theory and Practice. Springer, Wien, New York.

Kruse, L., 2001. Spatial and temporal distribution of atmospheric water vapor using space geodetic techniques. Geodätisch-geophysikalische Arbeiten in der Schweiz, Volume 61, Schweizerische Geodätische Kommision.

Mendes, V.B., 1999. Modeling the neutral-atmosphere propagation delay in radiometric space techniques. PhD dissertation, University of New Brunswick.

Mikhail, E.M., 1976. Observations and least squares. University Press of America.

Saastamoinen, J., 1972. Atmospheric correction for the troposphere and stratosphere in radio ranging of satellites. In *Henriksen, S.W.; Mancini, A.; Chovitz, B.H. (ed.): The use of artificial satellites for geodesy, Geophys. Monogr. Ser., AGU*, pp. 15:247–251.

SMA, 1985. Charakteristiken der ANETZ-Daten. In *Beiträge zum ANETZ-Daten Kolloquium vom 17. April 1985 in Zürich.*, p. 56. Schweizerische Meteorologische Anstalt Zürich.

Troller, M., 2004. GPS based Determination of the Integrated and Spatially Distributed Water Vapor in the Troposphere. Diss ETH No. 15513.

Troller, M., Bürki, B., Cocard, M., Geiger, A., and Kahle, H.-G., 2002. 3d refractivity field from GPS double difference tomography. *Geophys. Res. Let.*, 29(24), pp. 2149–2152.

Troller, M., Cocard, M., and Geiger, A., 2000. Modellierung 4 dimensionaler Refraktionsfelder zur Berechnung von Weglängen-Korrekturen bei Satellitenmessungen. In *Simulation raumbezogener Prozesse: Methoden und Anwendungen*, 9, *IfGI prints*.